Direct observation of the translocation mechanism of the transcription terminator Rho

Veronika Gocheva, Antoine Le Gall, Marc Boudvillain, Emmanuel Margeat, Marcelo Nollmann

Supporting information

SI 1. Tether design and single-molecule magnetic tweezers experiments on R_{H120}

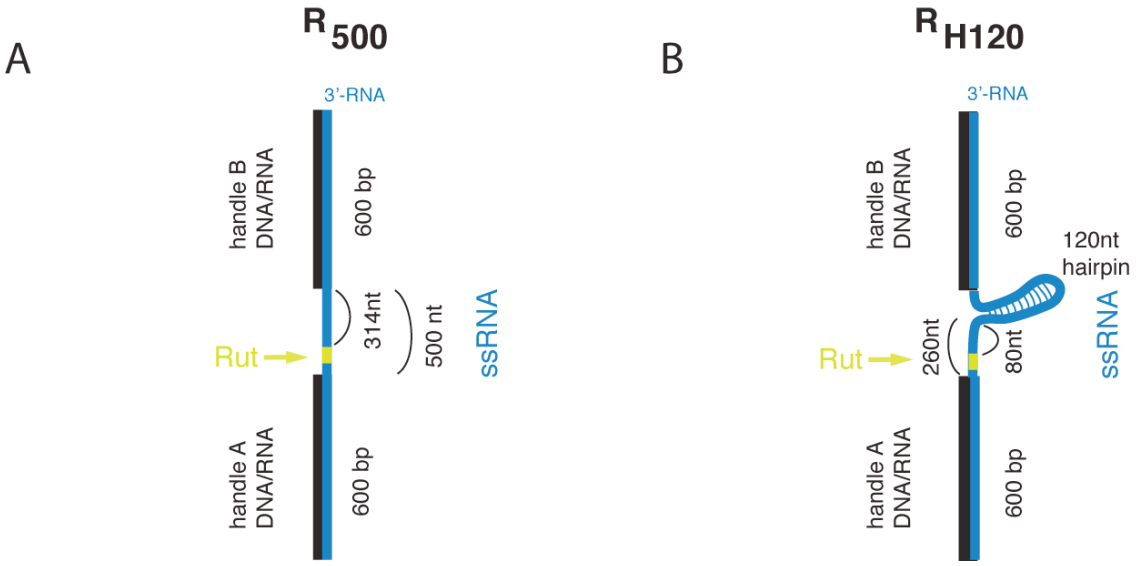

Supplementary Figure 1. Design of DNA/RNA tethers. Two tether constructs were used for investigating the translocation activity of Rho: R_{500} and R_{H120} (see Figure). The frequency of events, rates and processivities of Rho translocation observed in R_{500} and R_{H120} were indistinguishable within experimental error. Design, data, and best fit parameters for each tether are shown in Figure 2A and SI 5. The mean velocities and processivities shown in the main text are thus an average of all events. **(A)** In R_{500}, a 1.7kb-long single-stranded RNA molecule was annealed to two single-stranded DNA molecules (black lines) to form two regions of DNA/RNA hybrids, and a central, un-annealed, 500 nt-long ssRNA region (blue lines) (see Materials and Methods in main text). The Rut site (yellow) is located at 120 nt from the 5'-end of the central ssRNA, and at 314 nt from the 3' junction. **(B)** In R_{H120}, the ssRNA region contained a long, 120 bp hairpin 80 nt away from the Rut site (yellow). In both cases, the bottom DNA handle contained a biotin at its 3'end (used to attach it specifically to a BSA-biotin-coated coverslip surface pre-incubated with streptavidin) whereas the top handle contains a digoxygenin at its 5'end (used to specifically attach it to an anti-digoxygenin-coated magnetic bead).

SI 2. Schematic of λtR1 termination system.

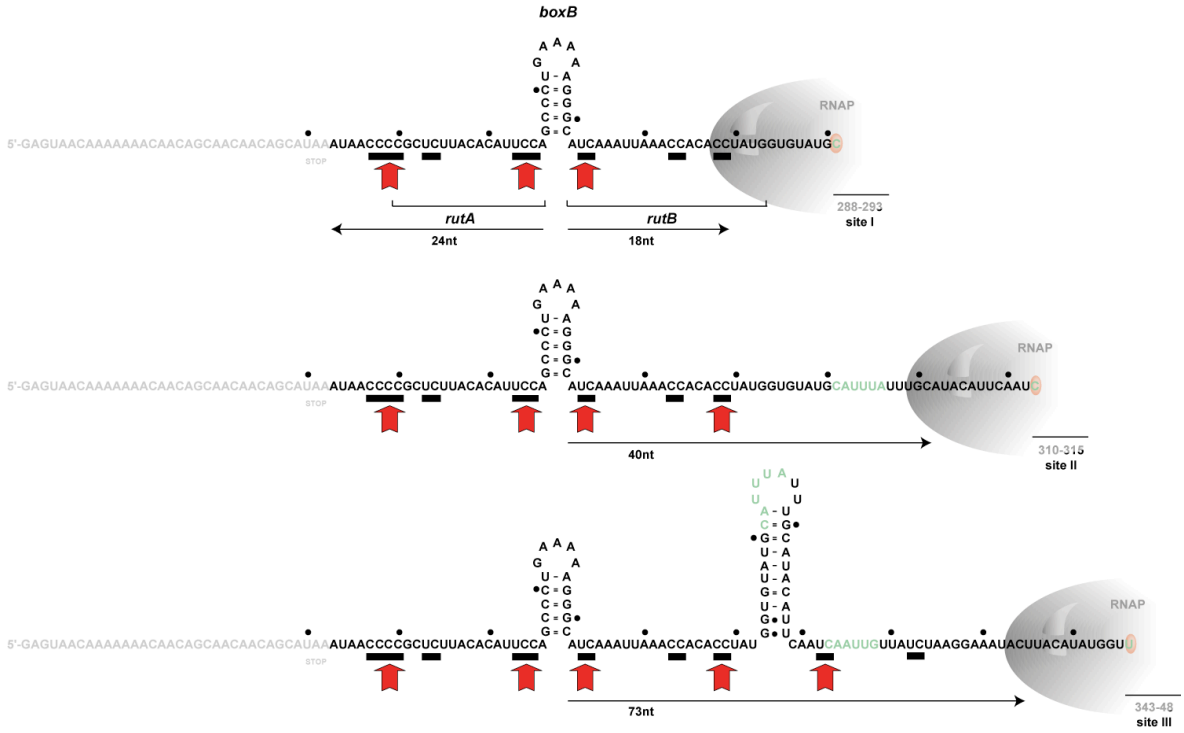

Supplementary Figure 2. Schematic of λtR1 termination system for the three clusters of transcript release sites (in green) (1-4). The upstream λcro coding sequence is shown in grey. The 5'-YC dimers in the RutA and RutB segments of theλtR1 Rut site that could be recruited by Rho PBS clefts are underlined. Note that, in *in vitro* experiments, additional anchoring points in the untranslated λcro region may be used by Rho ((5) and references within). The 3'-proximal transcript residue is shown in green within the polymerase active-site (in orange). The red arrows correspond to 5'-YC dimers whose spacing (>30Å) may allow concerted binding to a Rho primary binding site.

SI 3. RNA translocation by Rho in different tethers in the same field of view

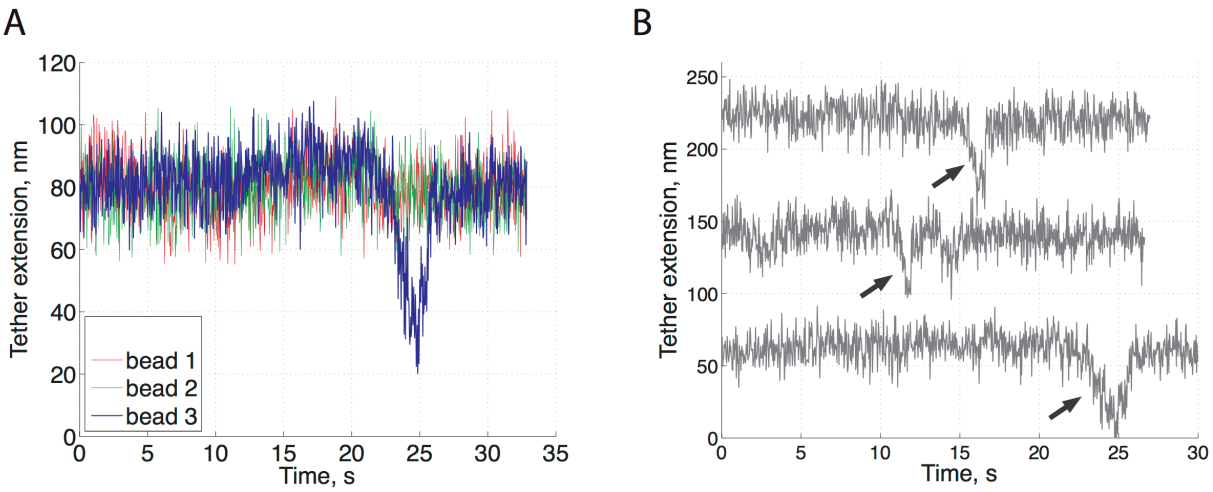

Supplementary Figure 3. Representative traces of the change in RNA extension due to single-molecule Rho activity. In our magnetic tweezers setup, several beads can be simultaneously tracked in 3 dimensions. (**A**) Typically, single events of Rho translocation appear in a single bead per field of view (as shown in the example in this panel). Panel A shows the activity of Rho on a single bead (bead 3, blue) in a field of view with several beads exhibiting no activity (beads 1-2, red and green). A pause after the RNA shortening event and before the release of the loop is shown. Raw data are displayed (34 Hz). Tether extensions represent relative, not absolute measurements of the tether length. (**B**) In this panel, we display several different single-molecule traces showing typical RNA shortening events observed only in the presence of Rho and ATP. Translocation rates and processivities were obtained as schematized in Figure 3C and described in Materials and Methods. Raw data are shown (34 Hz acquisition rate). For clarity, traces of other beads in the field of view are not displayed, and tether extensions were vertically shifted. Single-molecule shortening events are marked by arrows. In the majority of events (>85%), the RNA extension recovered instantaneously, as shown in Figure 3C, while in ~15% of events the recovery of extension was gradual.

SI 4. The affinity of Rho binding to RNA is not changed by nucleotide state.

To confirm that ADP and non-hydrolysable analogs trigger the same RNA binding and oligomerisation behaviors of Rho (6), we have now performed fluorescence anisotropy-based binding experiments with Rho and a labeled RNA substrate in the presence of ADP or non-hydrolysable AMP-PCP and observed no differences (see Figure below).

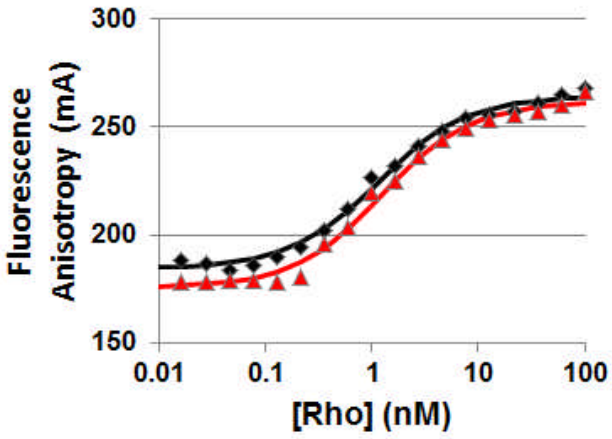

Nucleotide	ΔG (kcal / mol)
ADP	12.45 (± 0.1)
AMP-PCP	12.4 (± 0.15)

Supplementary Figure 4. Fluorescence anisotropy-based titration of a 132 nt RNA molecule labeled with Atto647N (at 0.5 nM) by Rho in presence of various nucleotides.

SI 5. Calculation of inhibition of initiation rates by an opposing external force

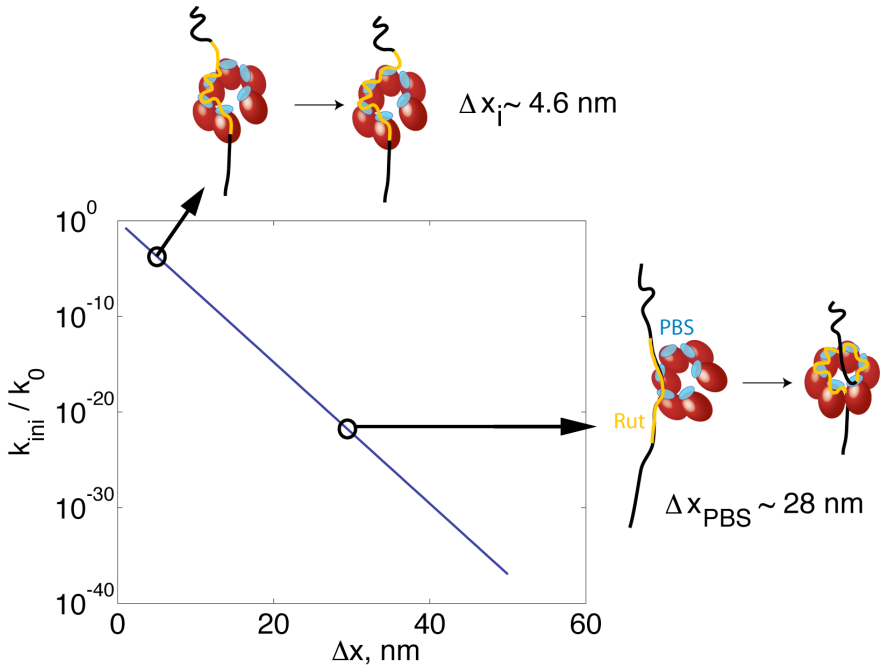

Supplementary Figure 5. Inhibition of binding rates by an opposing force. The assembly of an active Rho/RNA complex requires the multi-step wrapping of Rut around the PBS (several segments of Rut are bound to the six PBS in Rho), transient ring opening and closure, and an additional binding step of RNA to the SBS. Each of these wrapping and binding sub-steps produce a change in ssRNA extension and thus are susceptible to the tension on the RNA tether. The binding of the entire Rut site by the PBS produces a change in RNA extension of Δx_{PBS} ~ 28nm, with the reminder (Δx_{SBS}~ 17 nm) corresponding partially to binding to the SBS (7). Thus, we can estimate that, in average, the binding of Rut to each PBS in Rho produces a change in RNA extension of $\Delta x_{PBS,i}$ ~ 28 nm/6 ~ 4.6 nm. Assuming a simple transition state model (8), with a distance to the transition state of Δx, the rate of wrapping (a binding event producing a change in RNA extension and involving multiple protein-RNA contacts along the trajectory of the RNA tether) is given by :

$$k_{ini} = k_0 \, e^{-F\Delta x/kBT}, \qquad \text{Equation 1}$$

where k_0 is the rate at zero force, k_BT = 4.1 pN nm is the thermal energy of the bath, and F is the force applied to the magnetic bead. From this model, we can estimate the effect of 7 pN of opposing force in the rates of wrapping of each sub-step (Supplementary Figure 4). As expected, at 7 pN the shortening of RNA due to the additional binding to a single PBS site is mildly inhibited (~3 10^{-4}), whereas the rate of wrapping of Rut to the entire PBS is highly inhibited (~ 10^{-21}) (Supplementary Figure 5). The former inhibition ratio is similar to the inhibition of wrapping observed for other molecular motors, such as gyrase, in which case the wrapping of 31 nm of

DNA around gyrase at 1 pN of force inhibits the wrapping rate by a factor of 5 10^{-4} (9). In the case of gyrase, wrapping is required in each mechanochemical cycle, thus mild amounts of force have a direct effect on the processivity and initiation rate of the reaction. In contrast, wrapping of Rut by the PBS is not lost during translocation, therefore only the initiation rate, and not the processivity would be expected to be affected by force.

Due to intrinsic limitations in our magnetic tweezers setup, only binding events producing spontaneous changes in extension larger than ~10 nm are detectable. Thus, we are not able to detect the binding of individual binding sub-steps. These binding events are, in addition, infrequent (see above) and uncorrelated, thus even if their cumulative effect would produce a change in extension theoretically detectable (~28 nm), they become obscured by long-term drift and limited instrument resolution (see Supplementary Figure 6). In brief, our observations are consistent with Rho binding Rut in a step-wise manner, slowly and with extension changes undetectable in our setup (~ 5 nm). Thereby, at the beginning of an event of single-molecule RNA translocation by Rho, pre-association and assembly steps have already taken place. This interpretation is consistent with the low frequency of occurrence of translocation events observed in our experiments. In addition, we note that a recent study using force-spectroscopy showed that even when RNA is relaxed to zero force to promote Rho binding, most of the force-elongation curves do not display any Rho binding event (95%) (7).

A fundamental difference between Koslover's and our experiments lies in the moment when force is applied on RNA. In Koslover's setup, the Rho:RNA complex is formed at zero force and, then, an increasing force is applied on RNA to probe the transition energy barriers (in the form of 'rips' in extension versus force curves) along the Rho:RNA dissociation pathway. An important limitation of that configuration is that reaction time courses cannot be monitored directly. In our case, a constant tension on RNA (at least ~7 pN) was applied throughout the experiment (i.e., even before Rho was added) to "counter" Brownian motion and provide sufficient spatial resolution to monitor Rho-dependent tether extension changes in real time. An intrinsic limitation of this setup is that force-dependent reaction steps are kinetically slowed down, sometimes to the extent that they are impossible to detect unambiguously from instrumental noise.

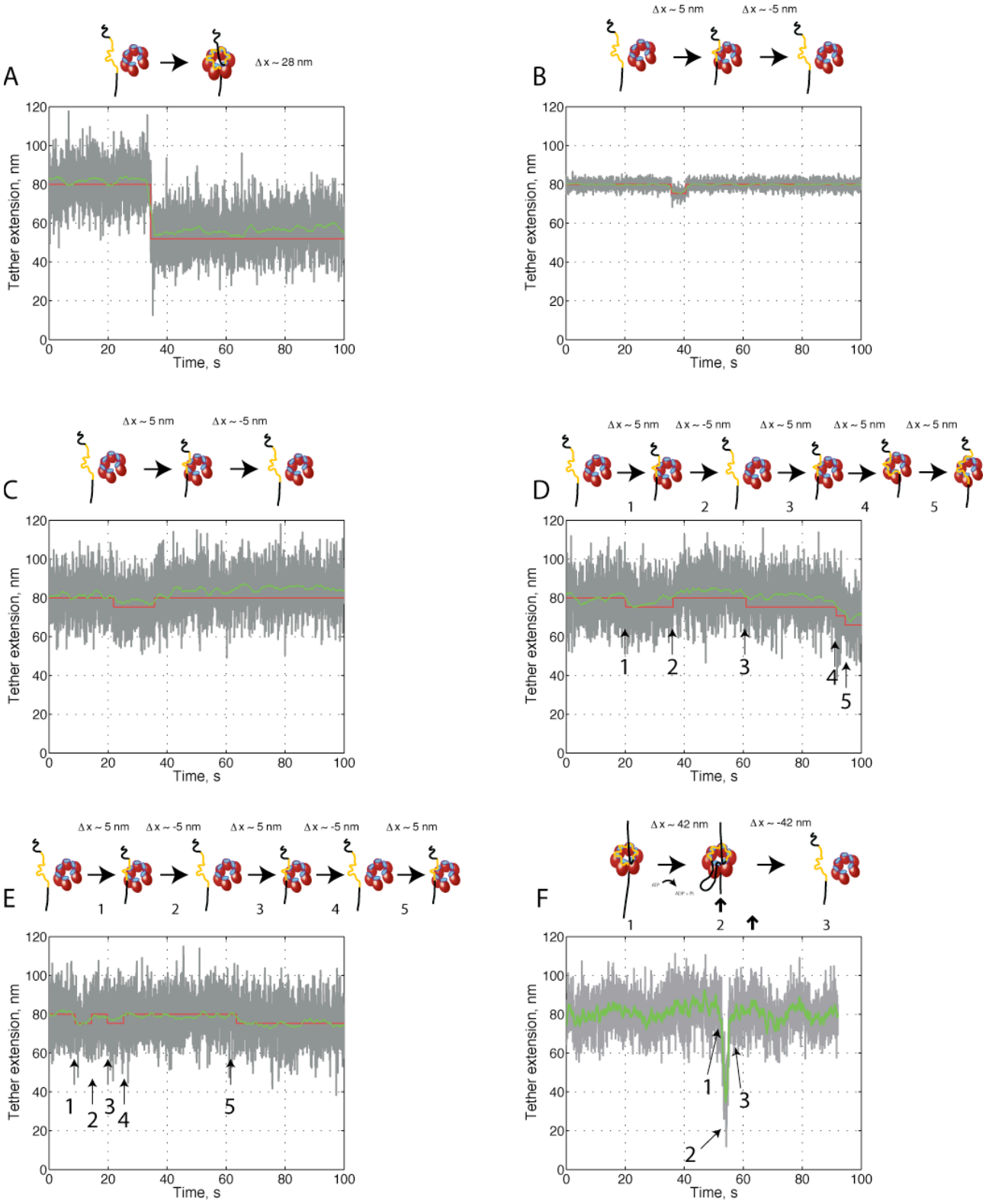
A
Δx ~ 28 nm
B
Δx ~ 5 nm
Δx ~ -5 nm
C
Δx ~ 5 nm
Δx ~ -5 nm
D
Δx ~ 5 nm
Δx ~ -5 nm
Δx ~ 5 nm
Δx ~ 5 nm
Δx ~ 5 nm
E
Δx ~ 5 nm
Δx ~ -5 nm
Δx ~ 5 nm
Δx ~ -5 nm
Δx ~ 5 nm
F
Δx ~ 42 nm
Δx ~ -42 nm
Tether extension, nm
Time, s

Supplementary Figure 6. Simulations to exemplify under which conditions wrapping of PBS by Rho may be observable by magnetic tweezers. We performed computer simulations to determine under which experimental conditions magnetic tweezers may be able to detect changes in tether extension corresponding to the wrapping of RNA to the full PBS, or a subset of PBS sites. To construct extension traces, each data point was randomly drawn from a gaussian distribution with standard deviation equal (A, C-E) to or better (B) than the resolution of our instrument. The baseline was very slowly shifted over time to simulate the small changes in experimental drift that cannot be corrected using our drift-correction algorithm (usually at time-scales of several minutes). RNA shortening events due to wrapping of RNA to each PBS site were simulated to happen instantaneously. Red lines show the extension of the tether without noise. Discrete changes in extension correspond to individual wrapping/unwrapping events. Grey curves correspond to raw data (34 Hz, same as the experimental frequency). Green curves correspond to a boxcar average of the data (1 Hz).

(A) Simulation of the cooperative binding of RNA to the full PBS. This would lead to an extension change (~28 nm) that should be experimentally detectable under our conditions and resolution. This large change in extension should happen independently of the presence of ATP. We did not observe these transitions under any condition in our experiments. This result is consistent with the very large inhibition (~ 10^{-21}) exerted by tension on the tether for such a large transition (see Supplementary Figure 5). Scheme of the simulated transition is shown on top.

(B) Simulation of the reversible binding of RNA to two consecutive PBS sites, at high experimental resolution. This event should lead to a change in extension of ~ 28/6 nm ~ 5 nm. As the simulation shows (green curve following the simulated red curve), this small change in extension would be detectable with an instrument resolution of 2 nm at 34 Hz (i.e. 0.34 nm/ √Hz). The rate of transitions is estimated as follows. The rate of nucleic acid wrapping under mechanical tension was reported to be ~10^3 Hz for DNA gyrase (wrapping of T-segment, interpolated to zero force) (9). Assuming a similar rate for Rho, and considering the inhibition due to tension on the tether (~10^{-4}, Supplementary Figure 5), we get an estimate of ~ 0.1 Hz at 7 pN. Scheme of the simulated transition is shown on top. These transitions are independent of ATP.

(C) Simulation of the reversible binding of RNA to two consecutive PBS sites, at our experimental resolution. At our instrument resolution (~10 nm at 34 Hz, i.e. 1.7 nm/√Hz), the binding of Rho to two consecutive PBS sites would not be resolved (compare grey and green lines with the simulated signal in red). Scheme of the simulated transition is shown on top. These transitions are independent of ATP.

(D) First example of a simulation of more complex transitions involving binding of RNA to a larger number of PBS sites. This would not be detectable under our experimental conditions either, as force inhibition spreads these transitions over time. Numbers indicate the position of each transition simulated in the trace. Scheme of the simulated transitions is shown on top. These transitions are independent of ATP.

(E) Second example of a simulation using the same conditions as in panel D. As in panel D, binding of RNA to PBS cannot be detected with our instrumental noise and due to the time separation between transitions.

(F) Experimental trace with a single translocation event. This kind of event was only observed in the presence of ATP. Raw data is shown in grey (34 Hz), and boxcar average in green (2 Hz). Small changes in tether extension similar to those expected from simulations can be observed before and after the active translocation event. These changes could correspond to partial wrapping of RNA to PBS. Unfortunately, due to the instrument resolution and the time scale of these changes, it is impossible to tell whether these correspond to instrumental noise or to real changes in RNA extension induced by Rho binding.

SI 6. Summary of rates and processivities of Rho in different tethers.

	R_{500}	R_{H120}	R_{500}+R_{H120}
mean velocity, gaussian fit	50 ± 4 nt/s	56 ± 4 nt/s	**56 ± 3 nt/s**
average velocity	59.6 ± 4 nt/s	62.8 ± 4 nt/s	61 ± 3 nt/s
mean processivity, gaussian fit	56 ± 4 nt	48 ± 4 nt	49 ± 3 nt
average processivity	62 ± 4 nt	61 ± 4 nt	**62 ± 3 nt**
number of events	35	27	62

Supplementary Table 1. Velocities and processivities of RNA translocation by Rho in R_{500} and R_{H120} obtained from fits to the distributions shown in Figure 4. In all cases, errors quoted represent the standard error of the mean (s.e.m.).

SI 7. Characterization of correct attachments in single-molecule fluorescence/ manipulation experiments.

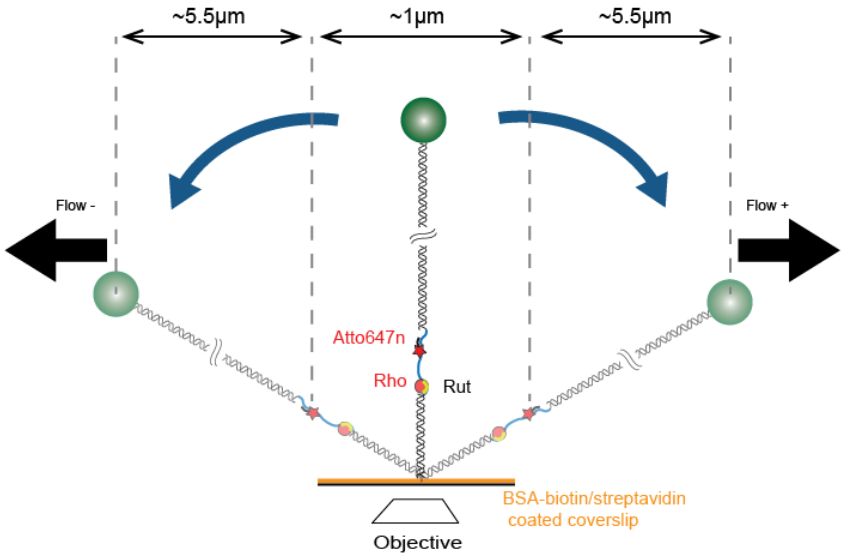

Supplementary Figure 7. The proper attachment of Atto 647N–labeled oligonucleotides on $R_{500\text{-}long}$ tethers was assessed by imaging the fluorophore while applying flow force in the forward and backward directions and measuring the distance between the two fluorophore positions and the distance between the bead and the fluorophore for the two flow directions (see Figure). This procedure was also used to assess whether the activity of Rho led to the displacement of the fluorescently-labeled DNA oligonucleotide after the period of incubation. Schematic representation of an experiment used to verify the proper attachment of the fluorescently-labeled oligonucleotide to the tether is shown in Figure. The fluorophore and the auto-fluorescence of the bead are imaged while applying flow force in the forward and backward directions. The estimated distance between the two fluorophore positions is estimated to be ~1 µm [(600 bp*0.34 nm/bp + 600 nt * 0.59 nm/ nt)*2 = 998 nm] while the theoretical distance between the bead (of radius 500 nm) and the fluorophore is ~ 5.5 µm (14700 bp * 0.34 nm/bp + 500 nm = 5498 nm).

SI 8. Oligonucleotides used in this study

Primers	Sequences
Primer 1	5’ AGCTGAATTCAAAGCGCGATCAACAAGGCCATTC 3’
Primer 2	5’ CAGTAAGCTTGCCGCCGGGCGTTTTTTATTG 3’
Primer 3	5’ TAATACGACTCACTATAGGGACTGGTGAGTACTCAACCAAGTC 3’
Primer 4	5’ TAGGAAGCAGCCCAGTAGTAGG 3’
Primer 5	5’ GCTTTAATGCGGTAGTTTATCACAG 3’
Primer 6	5’ Digoxigenin – GCATTAGGAAGCAGCCCAGTAG 3’
Primer 7	5’ GGAATTCCGACTGGTGAGTACTCAACCAAGTC 3’
Primer 8	5’ ATTCTTGAAGACGAAAGGGCCTCG 3’
Primer 9	5’ ACATTTCCCCGAAAAGTGCCA 3’
Primer 10	5’ GTTTCGCCACCTCTGACTTGA 3’
Primer 11	5’ Atto 647N – GCCGCCGGGCGTTTTTTATTGG 3’
Primer 12	5’ Phosphate – AATTTAGGAAGCAGCCCAGTAGTAGGTTG 3’
Primer 13	5’ Cy3 – GCCGCCGGGCGTTTTTTATTGG 3’
Primer 14	5’ TGGAATGTGTAAGAGCGGG 3’
Primer 15	5’ CAATAGGTGTGGTTTAATTTGAT 3’
Primer 16	5’ CATAGGTGTGGTTTAATTTGATGCCC 3’
Primer 17	5’ CTGGAATGTGTAAGAGCGGGG 3’
Primer 18	5’ GCCCTTTTTCAGGGCTGGAATGTGTAAGAGCGG 3’

Supplementary Table 2. Oligonucleotides used in this study

SI 9. Sequence of ssRNA regions used to generate R_{500} and R_{120}.

GGAAAGCGCGATCAACAAGGCCATTCATGCAGGCCGAAAGATTTTTTTAACTATAAACGCTGATGGAAGCG

STOP RutA

TTTATGCGGAAGAGGTAAAGCCCTTCCCGAGTAACAAAAAAACAACAGCATAAATAACCCCGCTCTTACAC

boxB RutB Stop I

ATTCCAGCCCTGAAAAAGGGCATCAAATTAAACCACACCTATGGTGTATGCATTTATTTGCATACATTCAAT

Stop II Stop III

CAATTGTTATCTAAGGAAATACTTACATATGGTTCGTGCAAACAAACGCAACGAGGCTCTACGAATCGAGA

GTGCGTTGCTTAACAAAATCGCAATGCTTGGAACTGAGAAGACAGCGGAAGCTGTGGGCGTTGATAAGTC

GCAGATCAGCAGGTGGAAGAGGGACTGGATTCCAAAGTTCTCAATGCTGCTTGCTGTTCTTGAATGGGGG

GTCGTTGACGACGACATGGCTCGATTGGCGCGACAAGTTGCTGCGATTCTCACCAATAAAAAACGCCCGGC

GGC

Supplementary Figure 8. DNA sequences of the 500 bp inserts coding for the ssRNA regions of the R_{500} construct. The *rut* site composed of *rutA* and *rutB* elements interrupted by the *boxB* structure are highlighted as well as *cro* gene translation stop codon and the three canonical transcription stop sites for this terminator. The Rut sites (RutA: violet and RutB: blue), interrupted by the boxB helix (olive), are highlighted. The three canonical stop sites for this terminator are highlighted in red.

260b-λtR1-120hp

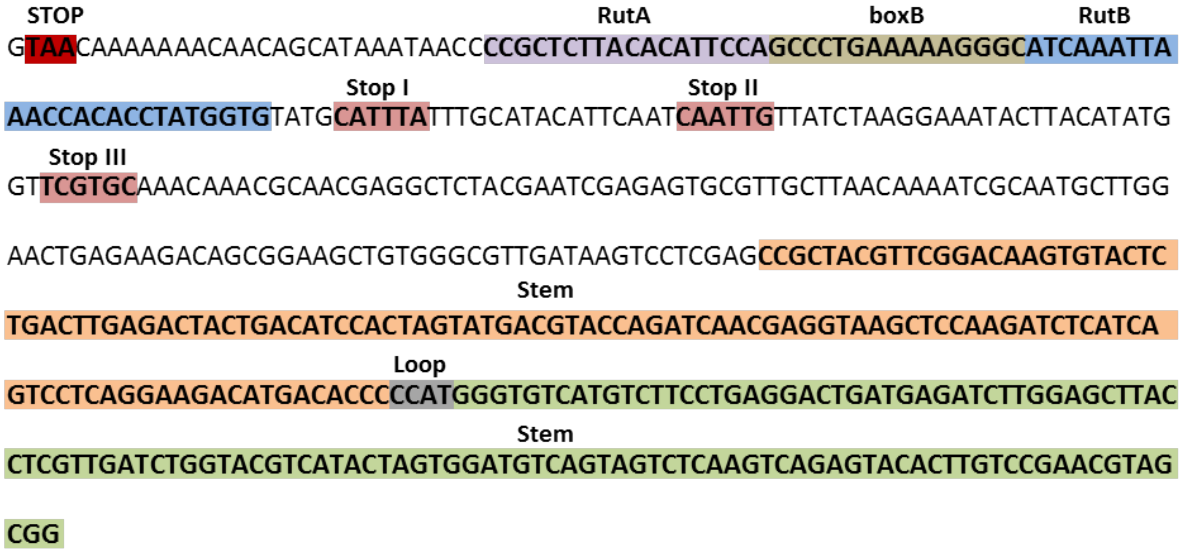

Supplementary Figure 9. DNA sequences of the 500 bp inserts coding for the ssRNA regions of the R_{H120} construct. The Rut site (RutA: violet and RutB: blue), interrupted by the boxB helix (olive), are highlighted. The three canonical stop sites for this terminator are highlighted in red. The 240 bp inverted repeat of the R_{H120} construct is highlighted in orange and green.

SI 10. Preparation of RNA tethers.

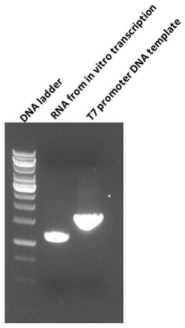

Supplementary Figure 10. Preparation of RNA tethers was performed as described in the Materials and Methods section. Briefly, the ssRNA region to be tethered between RNA/DNA handles (see SI 1) was cloned into pBR322. This template was then used to produce a ~1.7 kbp ssRNA transcript by *in vitro* transcription and its purity and homogeneity was verified by gel electrophoresis. Figure shows a gel migration of the RNA produced by *in vitro* transcription using pBR322-λtR1 (middle lane) and the PCR-amplified double-stranded DNA from the T7 promoter to the end of handle B (right lane).

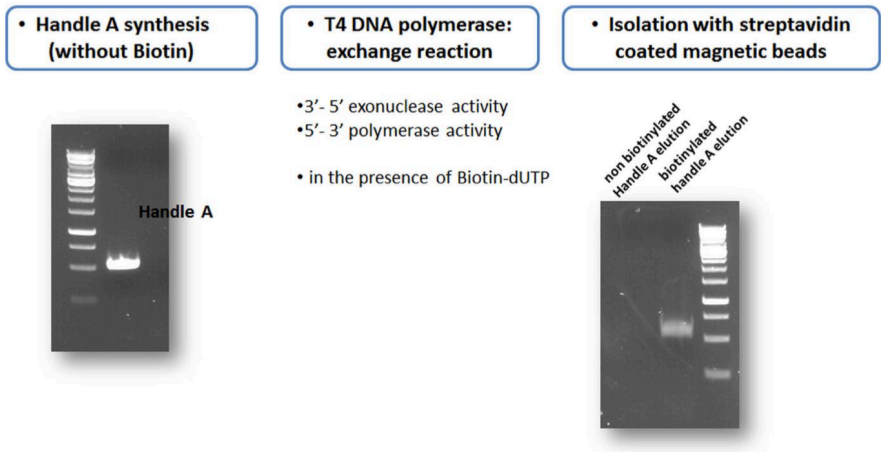

Supplementary Figure 11. Handle A was produced by PCR amplification and a biotin attached to its 3'-end by using T4 DNA polymerase. Biotinylation of handle A : non-labeled handle A was first produced by PCR amplification (left). A T4 polymerase reaction was performed exhibiting 3'-5' exonuclease activity and 5'-3' polymerase activity in the presence of biotin-dUTP (middle). Biotinylation efficiency was verified by incubating the biotinylated and the non-labeled handles with streptavidin-coated magnetic beads. The DNA handles were eluted only for the fraction corresponding to the biotinylation reaction.

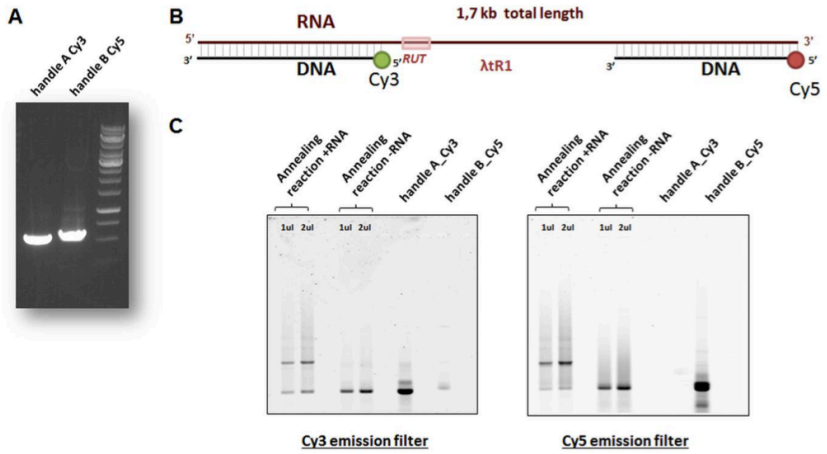

Supplementary Figure 12. Biotinylation efficiency was verified by purification using streptavidin-coated magnetic beads by quantifying the annealing reaction with Cy3/Cy5 labeled DNA handles. **(A)** DNA handles A and B were amplified with Cy3 and Cy5 labeled primers, respectively. **(B)** Schematic representation of the construct produced with the two labeled DNA handles after annealing. (**C)** Handle B was produced by PCR amplification using a 5'-digoxygenin-labeled primer. Both handles were annealed with the ssRNA fragment to obtain tethers. Assembly of tethers was followed by attaching a Cy3 to the 5'end of handle B and Cy5 to the 5'-end of handle A by PCR amplification and monitoring the formation of molecules with a lower mobility and containing both dyes. After gel migration, the annealing reactions performed with the labeled handles and with or without RNA, were scanned for Cy3 and Cy5 fluorescence emission. The labeled DNA handles alone were also submitted to gel migration as a control. When the annealing reaction is performed with RNA a lower mobility band showing Cy3 and Cy5 fluorescence and corresponding to the tether showed in panel B is formed (first two bands in gels).

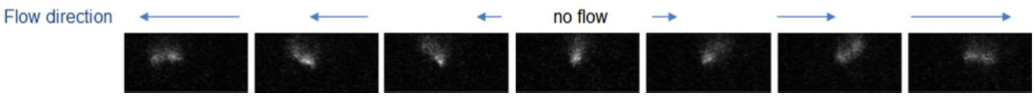

Supplementary Figure 13. To further verify the integrity of the RNA tethers, we used total internal reflection microscopy (TIRFM) to directly visualize surface-attached tethers by the fluorescence emission of intercalating dye (YOYO-1). The surface was passivated using a polyethylene glycol brush and tethers were specifically attached by streptavidin-biotin interactions. Under these conditions, the estimated tether extension was 900 ± 70 nm, consistent with the expected tether length when taking into account the ~50% length increase of the DNA/RNA handles due to intercalation (1200 bp * 0.34 nm/bp * 1.5 + 500 nt * 0.59 nm/nt = 907 nm). In these experiments, the center of the tether shows a lower fluorescence intensity (see Figure) in agreement with a poor labeling of the single-stranded region by the intercalating dye. In Figure, the R_{500} construct,

tethered to the surface of the reaction chamber, is imaged after labeling with the YOYO-1 intercalating dye (see Figure). The tether is imaged while the direction of the flow is changed from left to right.

SI References

1. Faus, I. and Richardson, J.P. (1990) Structural and functional properties of the segments of lambda cro mRNA that interact with transcription termination factor Rho. *J. Mol. Biol.*, **212**, 53–66.

2. Graham, J.E. and Richardson, J.P. (1998) rut Sites in the nascent transcript mediate Rho-dependent transcription termination in vivo. *J. Biol. Chem.*, **273**, 20764–20769.

3. Lau, L.F., Roberts, J.W. and Wu, R. (1982) Transcription terminates at lambda tR1 in three clusters. *Proc. Natl. Acad. Sci. U.S.A.*, **79**, 6171–6175.

4. Morgan, W.D., Bear, D.G. and Hippel, von, P.H. (1983) Rho-dependent termination of transcription. I. Identification and characterization of termination sites for transcription from the bacteriophage lambda PR promoter. *J. Biol. Chem.*, **258**, 9553–9564.

5. Rabhi, M., Espéli, O., Schwartz, A., Cayrol, B., Rahmouni, A.R., Arluison, V. and Boudvillain, M. (2011) The Sm-like RNA chaperone Hfq mediates transcription antitermination at Rho-dependent terminators. *EMBO J.*, **30**, 2805–2816.

6. Gan, E. and Richardson, J.P. (1999) ATP and other nucleotides stabilize the Rho-mRNA complex. *Biochemistry*, **38**, 16882–16888.

7. Koslover, D.J., Fazal, F.M., Mooney, R.A., Landick, R. and Block, S.M. (2012) Binding and translocation of termination factor rho studied at the single-molecule level. *J. Mol. Biol.*, **423**, 664–676.

8. Wang, M.D., Schnitzer, M.J., Yin, H., Landick, R., Gelles, J. and Block, S.M. (1998) Force and velocity measured for single molecules of RNA polymerase. *Science*, **282**, 902–907.

9. Gore, J., Bryant, Z., Stone, M.D., Nollmann, M., Cozzarelli, N.R. and Bustamante, C. (2006) Mechanochemical analysis of DNA gyrase using rotor bead tracking. *Nature*, **439**, 100–104.